Infrared thermography in metallic environments of WEST and ASDEX Upgrade

M-H. Aumeunier [a,*], J. Gerardin [a], C. Talatizi [a], M. Le Bohec [c], M. Ben Yaala [b], L. Marot [b], T. Loarer [a], R. Mitteau [a], J. Gaspar [c], F. Rigollet [c], X. Courtois [a], M. Houry [a], A. Herrmann [d], M. Faitsch [d], the WEST team[1], and ASDEX Upgrade team

[a] CEA Cadarache, 13108 Saint Paul-Lez-Durance, France
[c] Aix Marseille Univ, CNRS, IUSTI, Marseille, France
[b] Department of Physics, University of Basel, Klingelbergstrasse 82, 4056 Basel, Switzerland
[d] Max-Planck-Institut für Plasmaphysiks, D-85748 Garching, Germany

A B S T R A C T

Infra-red (IR) thermography is a widely used tool in fusion devices to monitor and to protect the plasma-facing component (PFC) from excessive heat loads. However, with the use of all-metal walls in fusion devices, deriving surface temperature from IR measurements has become more challenging. In this paper, an overview of infra-red measurements in the metallic tokamaks WEST and ASDEX Upgrade (AUG) is reported and the techniques carried out in the modeling and experimental fields to deal with this radiative and fully reflective environment are presented. Experimental characterizations of metallic samples in laboratory and experiments in WEST and AUG reveal that the behavior of both the emission and the reflectance can vary significantly with surface roughness, machining process and as the plasma operation progress. In parallel, the development of a synthetic IR diagnostic has allowed for a better interpretation of the IR images by assessing the reflection patterns and their origin. This has also proven that small-scale change in the emission pattern of beveled PFC can be confused with abnormal thermal events. Numerical solutions to evaluate the contribution of the reflections associated with a variable emissivity in a fully reflective and radiative environment are finally presented.

1. Introduction

In magnetic fusion devices, the vessel walls receive high heat and particle loads. The performances of the plasmas strongly depend on the ability to simultaneously monitor and control the plasma-wall interaction for protecting the walls from excessive heat loads. Infra-red (IR) measurement is a very appropriate method which fulfills such requirements, by providing thermal images of the Plasma Facing Components (PFC) under plasma exposure [1–3]. This IR technique has been demonstrated to be a reliable tool for both physics studies and real-time monitoring of PFCs with carbon PFCs. Nevertheless, in today's fusion devices, with the introduction of all-metal walls, additional difficulties result in the interpretation of IR measurements through disturbance phenomena such as reflections, and/or emissivity variation with surface temperature and plasma exposition (surface erosion/deposition on monitored PFCs). This can lead to inaccurate PFC surface temperature estimation and interpretation of "false hot spots".

In this paper, an overview of techniques developed for infra-red

measurements in the metallic tokamaks WEST [4] and ASDEX Upgrade (AUG) [5] is reported. First, a synthetic diagnostic has been developed to predict the IR measurement accurately in a fully reflective and radiative environment, as described in Section 3. In parallel, experimental characterizations of metallic samples with different roughness have been first carried out to establish a comprehensive model of emission and reflectance as a function of the temperature, the wavelength and the observation direction. The first results are presented in Section 4. The comparison between the expected heat load pattern and the associated surface temperature through the modeling and the experimental results is reported for experiments on WEST and AUG in Section 5. The approach and the issues related to the quantitative IR thermography in such a harsh environment is discussed in Section 6. Numerical solutions under investigation are presented prior to the conclusions.

---

2. Infra-red measurement in metallic fusion devices

In fusion devices, the IR thermography system addresses two main functions: its primary role is to ensure the machine protection by monitoring the surface temperature of the PFCs exposed to high heat flux. The second one aims to study the wall-plasma interaction for a better understanding of plasma edge, PFC aging and optimization of plasma scenario. As a result, the level of analysis of these two functions and the required accuracy is not the same. Machine protection function requires an entirely reliable method for real-time monitoring and feedback control to Plasma Control System for avoiding PFC damaging, crack and/or water leak. Physics studies need an excellent knowledge of the heat load pattern for assessing the physical phenomenon. Besides, more and more IR cameras aiming at monitoring the maximum surface of in-vessel components are used in fusion devices. Typically, WEST uses 12 IR cameras [6], whereas ITER plans 21 cameras [7]. With the increase of data to be analyzed, an automatized and robust wall monitoring system will also be needed to assist the wall protection officers. However, the optical radiative properties of metallic components make more complicated IR measurements. Due to the low emissivity of metallic targets and the heterogeneous radiative surrounding, the surface temperature measurement of the targets is not "direct" as for carbon, which emissivity was high enough for considering the potential reflected flux as negligible. Indeed, the total flux collected by the camera includes both an emission part coming from the target and directly related to the target temperature and an additional signal coming from the multiple reflections of the radiative surrounding. This has consequences both on the qualitative analysis with the presence of "false hot spot" in the image that could trigger false alarms, and so limiting the achievement of high performances plasma scenario, and on the quantitative analysis leading to overestimation of the surface temperature. Fig. 1 illustrates the impact of the contribution of the reflected flux in the collected flux on the measured temperature of a target of 0.2 emissivity. These estimations are based on a simplified numerical model considering a 2-surface enclosure made of (1) a flat surface of $S_{div} = 7\,m^2$ representing the divertor (target) and (2) an enclosed surface of $S_{wall} = 83\,m^2$ representing the vacuum vessel with an emissivity of 0.3. The radiative heat exchange between these 2 enclosure surfaces is computed from radiosity equations assuming diffuse, gray, opaque and uniform radiative surfaces. Preliminary findings emerge: considering

wall temperature of 200 °C, temperature measurement accuracy of a hot target (>400 °C) is dominated by emissivity variation with a risk of underestimation of temperature whereas temperature measurement of a colder target (<400 °C) is also affected by parasitic light coming from multiple reflections. This behavior can especially impact the analysis of the heat flux decay length measurement in "cold" regions. Up to now, there is no mature technique able to solve emissivity variation and reflection contribution. This paper presents a numerical approach to get a more reliable infra-red measurement.

3. Infra-red synthetic diagnostic

An IR synthetic diagnostic, designed as a "digital twin", has been developed to predict infra-red measurement in metallic environment: an "end-to-end" simulation aiming to model all physical phenomenon involved in the IR measurement chain, from the IR source to the optical response of the instrument. This includes (1) the modeling of the IR source, coming from the plasma heat loads deposited on PFCs, (2) the modeling of materials optical radiative properties which manage the photon-wall interaction through emissivity and reflectance models and (3) the optics modeling, including the camera model to reproduce the sensor image and the optical transfer function to take into account optics effects like diffraction and aberrations. All these models are used as input of Monte Carlo Ray tracing code (of ANSYS-SPEOS company [8]) using random process to predict rays behavior into 3D complex geometry. Backward ray tracing algorithm (when ray starts from eye or camera to light source) is used to provide the collected flux per pixel of an IR image. The accuracy of simulated data will depend on the number of rays N launched from pixel ($\sim 1/\sqrt{N}$). Regarding the IR source modeling, a field line ray-tracing code based on optical approximation [9] is used to compute the 3D field of deposited heat flux on WEST divertor from a given magnetic equilibrium. The resulting 3D temperature field used as input of photonic simulation is then computed from fast thermal reduced model based on modal identification method [10,11]. Such an original method is an alternative to finite element method (FEM) method able to solve thermally huge 3D geometry within a reduced calculation time and without losing accuracy (including 3D thermal diffusion, thermo-dependent properties). For AUG, there is no field line ray tracing code to predict the deposited heat flux on divertor, used as input of photonic simulation. The 3D thermal scene observed by
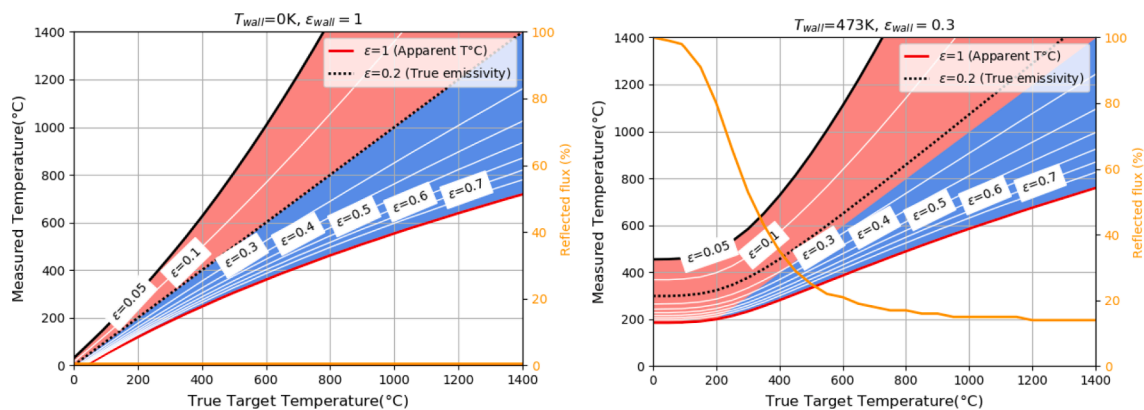

Fig. 1. Surface temperature measured in the Middle Wavelenght IR ($\sim 4\,\mu m$) region as a function of the true surface temperature of the target with an emissivity of 0.2 (Left Figure) no radiative environment (wall temperature $T_{wall} = 0\,K$) and without reflected flux (wall emissivity $\varepsilon_{wall} = 1$). The error only comes from the target emissivity imprecision. On the right figure, surface temperature evaluation with the contribution of the reflected flux. In this case, the errors come from target emissivity imprecision and additional parasitic light. Orange curve shows the part of reflected flux (parasitic flux) within the total flux collected by camera ($\sim 80\%$ at 200 °C, 20% at 600 °C). The blue area indicates the case when the measured temperature overestimates the true temperature (without risk for machine safety but limiting plasma scenario development causing false alarms), red area when the measured temperature underestimates the true temperature (with a risk to damage wall components) . The red curve is the apparent temperature (or blackbody temperature) measured by default by IR thermography system, namely when an emissivity of 1 is considered. The dotted black curve is the measured temperature when target emissivity (0.2 here) is known and corrected: in the first case, the true temperature is well recovered, whereas in the second case, the measured temperature is overestimated because of additional parasitic light. (For interpretation of the references to colour in this figure legend, the reader is referred to the web version of this article.)

synthetic diagnostic is then reconstructed from AUG experimental image obtained with high resolution camera focused on one divertor tile. A 2D to 3D projection mapping is used for getting temperature distribution on one tile and axisymmetry is assumed for getting 3D temperature field on the whole divertor. If such a process is not sufficient for quantitative comparison (this would require absolute experimental temperature map), this is consistent for qualitative comparison between simulated and experimental images and identify the main reflections patterns as shown in Section 5.1.

4. Experimental characterization of materials thermal optical properties

The thermal optical properties of an opaque material describes, through the emissivity, how much light is radiated from the material compared to the amount radiated by a blackbody at the same temperature and through the reflectance, how much light is reflected from a surface to the total incident radiant flux. For an opaque material (i.e., transmission $= 0$), the spectral (λ) directional(') hemispherical ($\cap$) reflectivity $\rho_\lambda^{'\cap}$ and spectral directional emissivity ε'_λ are linked by the Kirchhoff's law: $\varepsilon'_\lambda = 1 - \rho_\lambda^{'\cap}$. A set of experiments have been conducted in order to get a full initial description of these thermal optical properties of materials used in tokamaks. The objective is to understand and to anticipate how these properties change with the wavelength, the temperature and the roughness. In a first step, four tungsten (W) reference samples polished with different roughness (from 55 to 1120 nm) have been characterized in reflectance and emittance at room temperature in the spectral range [200–2500 nm] and compared to W samples coming from providers of WEST Plasma Facing Unit (PFU) [12].

4.1. Reflectance measurement

The total reflectance is subdivided into diffuse reflectance and glossy components, as illustrated in Fig. 2. For measuring and describing the sample reflectance fully, complementary experimental testbed operating at room temperature have been performed as described in [12]. The directional hemispherical (total) reflectance $\rho_\lambda^{'\cap}$ and the diffuse part $\rho'_{\lambda,diff}$ are measured with an integrating sphere of Varian Cary spectrophotometer. The angular dependence of reflectance is measured with a goniometer which provides the bidirectional reflectance $\rho_\lambda^{''} = \rho_\lambda(\theta_i, \varphi_i, \theta_r, \varphi_r)$ with (θ_i, φ_i) and (θ_r, φ_r) respectively angles of incidence and reflection. Fig. 3 shows an example of measured bidirectional reflectance for one of the W reference sample with a roughness of 1120 nm. For all W reference samples, the reflectivity follows a Gaussian distribution with increasing intensity at a higher incident angle. The Full Width at Half Maximum (FWHM) of the Gaussian specular lobe is minimal from 1 to 9° as a function of roughness and relatively constant with wavelength.

4.2. Emittance measurement

Spectral normal emissivity is measured from three testbeds. The first one relies on direct measurement of emissivity, comparing the sample emission heated within vacuum vessel with blackbody emission collected by IR camera as described in [13]. The two other ones rely on

indirect measurement using integrating sphere for visible and near-IR range and Fourier Transform Infra-red Spectrometer systems for IR range to measure spectral total reflectance of samples at room temperature. The spectral normal emissivity is then inferred using Kirchhoff's Law. The results of the three testbeds are gathered in Fig. 4 (Left), which describes the spectral normal emissivity value for several W samples with different roughness. The experimental results are quite coherent with theoretical models [14] with a significant decrease of the emissivity with wavelength and an increase of the emissivity with sample temperature. The strongest dependence is on the wavelength with a drop by a factor 5 from visible to IR range ($\sim$4 µm). However, the temperature dependence is low (and almost linear) with an increase of emissivity of 0.04 for a temperature increase about 600 °C which is in line with the Hagen Rubens model [15]. There is also a good agreement of the measured emissivity of W samples from the different testbeds exhibiting a W emissivity value around 0.1–0.2 at 4 µm. At this stage, for IR image interpretation, it is also essential to keep in mind that the materials emission model is also characterized by the intensity diagram emission, which describes the angular dependency of emissivity as illustrated in Fig. 4 (Right). The angular dependence is described with a cosine n power model with n $= 1$ for Lambertian distribution, with n > 1 for directional emission and n < 1 for grazing emission. This will impact the IR interpretation by increasing or decreasing measured thermal emission as a function of the observation angle and camera resolution. The angular-dependency of emissivity ε'_λ has been measured through an indirect method from the measurement of the spectral directional hemispherical reflectance $\rho_\lambda^{'\cap}$ described in Section 4.1 and following to Kirchhoff's Law $\varepsilon'_\lambda = 1 - \rho_\lambda^{'\cap}$. In the visible range, the n coefficient is found between 0.6 and 1 depending of the wavelength favoring grazing angle. In the IR range, n close to 1 can be extrapolated by fitting theoretical models from experimental data in visible and near-infrared range; however, this needs to be measured.

Regarding the question on the roughness dependency, for W very polished samples, the main trend shows an increase of the emissivity with the roughness except for the sample with 180 nm roughness which has different optical constant (refractive index n and extinction coefficient k). However, additional effects from the machining process, the presence of scratches, grooves, cracks will change the emissivity and reflectance model, and in this case, the roughness parameter is no longer sufficient to fully explain and describe the thermal optical behavior. This has been confirmed with the observation of unpredicted light patterns on a WEST PFU fillet coming from a change of emittance model between the PFU top face and fillet (Section 5.2.)

5. Infra-red measurements in WEST and ASDEX Upgrade

5.1. Discriminate reflection features from real thermal events

The first point to be solved from IR measurement is to discriminate real thermal events from "false hot spots" which are not a risk for machine safety. Realistic simulation of photon behavior in a fully radiative and reflective environment is an essential tool to identify reflection patterns and to know their origin. Fig. 5 shows the experimental image of WEST wide-angle tangential view compared to the simulated images in the case considering high specular reflectance model (Fig. 2b) fitting to laboratory measurement of W samples as described in Section 4.1. and

Fig. 2. The full Bidirectional Reflectivity Distribution Function (BRDF) is described as the sum of diffuse component (A) and glossy components for sharp (B) and blurry (C) components.
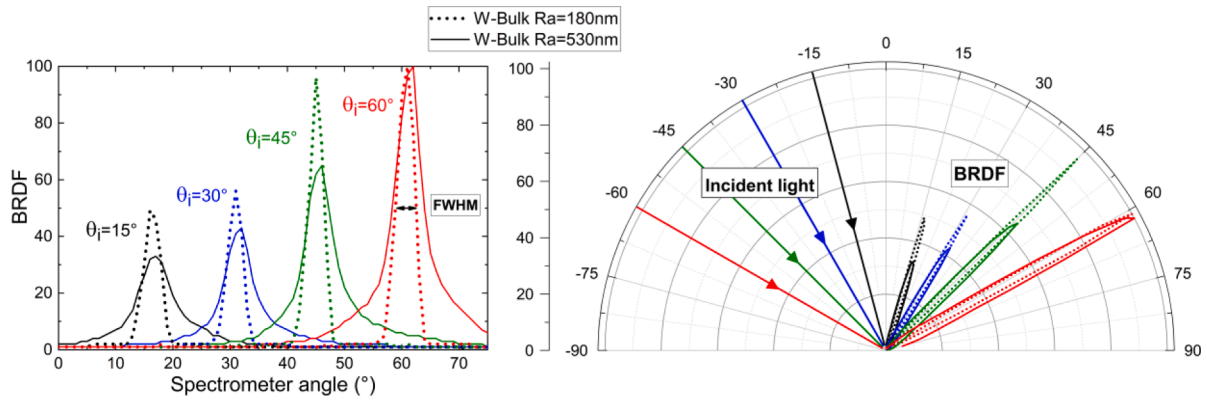
Fig. 3. Example of measured bidirectional reflectance of a W-Bulk sample at Ra = 180 nm and Ra = 530 nm for λ = 900 nm following two representation in cartesian coordinates (left figure) and in polar coordinates (right figure): reflectivity follows a Gaussian distribution around the theoretical specular direction according to the Snell-Descartes law and with increasing intensity at higher incident angle. The Full Width at Half Maximum (FWHM) of Gaussian increases with roughness.
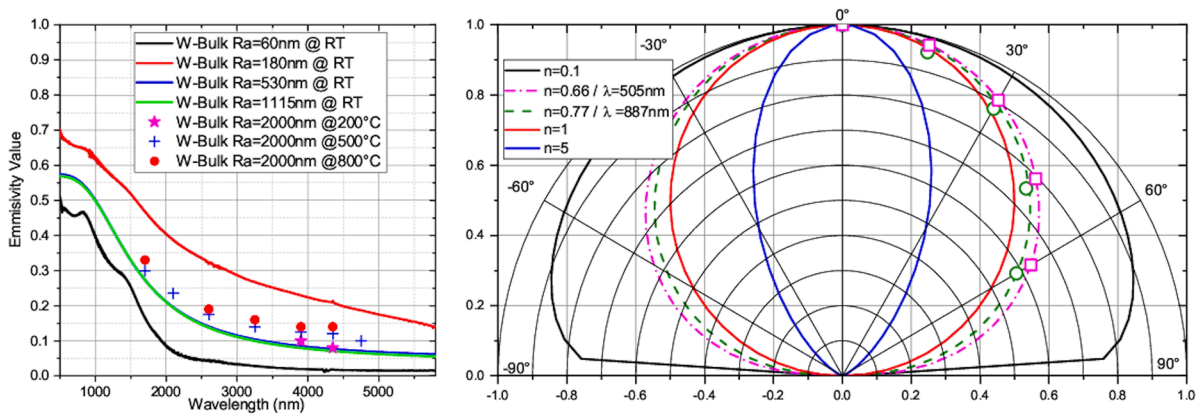

Fig. 4. (Left Figure) Spectral normal emissivity as a function of wavelength for different reference bulk-tungsten samples with different roughness and measured at Room Temperatrure (RT). W-Bulk Ra = 2000 nm come from WEST PFU manufacturers. (Right Figure) Intensity diagram emission describing the emissivity angular dependency as a cosine n-power model with n = 1 for Lambertian distribution, n > 1 for direction emission, and n < 1 for grazing emission. Dashed curves show measured (normalized) directional emissivity and n power fitted for sample W-bulk Ra = 530 nm at 500 nm and 900 nm.
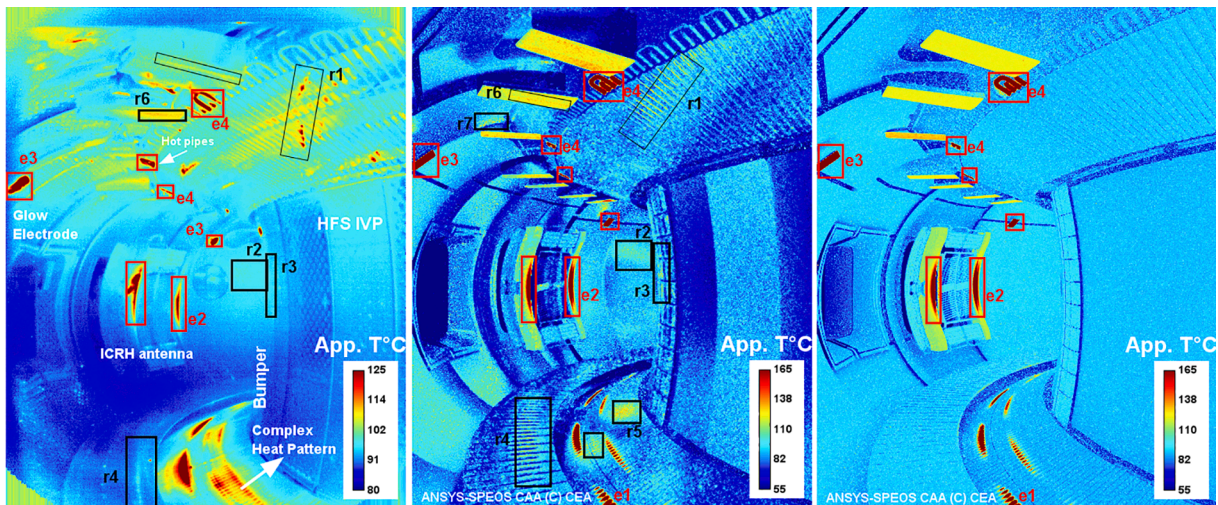

Fig. 5. (Left figure): Experimental IR image (in brightness temperature) of WEST wide-angle tangential view (Pulse #55210) (Middle image) Simulated image considering high specular reflectance model roughly fitting to laboratory measurement (Right image) Simulated image considering diffuse reflectance model. Red rectangles annoted ei (e for emission and i region number) correspond to hot spot (e1: divertor heat load, e2: heat load on antenna outboard, e3: glow electrode, e4: hot upper pipes). Black rectangles annoted ri (r for reflections) correspond to reflections features (r1-r2: reflections from low divertor, r3-r6: reflections from ICRH outboard, r7: reflections from upper ripple protections). (For interpretation of the references to colour in this figure legend, the reader is referred to the web version of this article.)

in the case considering all diffuse surfaces (Fig. 2a). Definitely, specular surface models on WEST wall surface fit with experimental images in accordance with measurements of reference samples. The brightness temperature map is quite uniform in case of a diffuse surface, whereas the specular case reproduces a specific light pattern as experimentally observed. To analyze in detail IR image, first considering the main and well-known heat loads used as input of photonic simulation: there are (i) the heat loads on lower divertor and antenna outboard coming from conducted particles along magnetic field lines and modeled by PFCFLUX code [9], (ii) the hot upper pipes exposed to fast electrons escaping from plasma [16] and (iii) glow electrodes not actively cooled. It is worth noting that a complex heat load pattern on the inner lower divertor is observed in the experimental image: its origin is under investigation (splitting inner-strike-point divertor, emissivity change along the poloidal direction, or both). A large number of hot spots on the WEST wide-angle IR view originate from the outboard ICRH (Ion Cyclotron Resonance Heating) antenna protection limiters to upper part of the First Wall, on baffle, lower divertor and bumper and from the lower divertor to upper divertor and outer wall.

Fig. 6 shows the experimental and simulated image of AUG IR camera [17], assuming high specular reflectance models ($\varepsilon \approx 0.2$, i.e., 80% reflectance with 2% of diffuse reflectance). The main reflection patterns are quite well reproduced and identified on the outer dome originating from the outer target, on the outer lower divertor and inner dome coming from the inner target and on inner lower divertor coming from the outer target. Secondary reflections (light hitting two surfaces before being collected by the camera) are, in this case quite present on the outer and inner target. It is worth noting that, contrary to WEST, the closed geometry of AUG divertor (target facing each other's as in the ITER divertor) makes the reflections patterns more complex and challenging to anticipate intuitively due to the multiple reflections. The anticipation of reflection patterns become susceptible to strike point position and tiles misalignment. Regarding the hot spots not captured by simulation, especially on outer target, simulation proves that these are not reflection patterns but these may be due to another physic phenomenon under investigation such as local change of emissivity, object misalignment or another heat source (such as heat losses) not still modeled.

5.2. Impact of emissivity model on IR measurement

Unexpected light pattern (not predicted by field line tracing code) has been observed along the rounded bevel of WEST inertial PFU (trailing edge) from several infra-red cameras, as shown in Fig. 7. To explain and understand the origin of recurring light pattern on PFU, several hypotheses have been studied with simulation. The first assumption excluded by IR modeling is a reflection pattern. Several possible reflection contributions have been investigated as shown in Fig. 8: (1) light coming from adjacent PFU at 400 °C and reflected by bevel, (2) multiple reflections between lateral faces of PFU at 70 °C and (3) other contributions coming from in to vessel components out of camera views. The part of reflected flux, on the region where is localized the light pattern, is estimated by simulation between 5 and 20% depending on the position along the bevel, which is, in all cases, not significant enough for reproducing light pattern as observed on IR camera. The luminous trail is in fact, reproduced by decreasing the normal emissivity value and/or increasing of grazing emission of the top face compared to the fillet surface (Fig. 9). This proves that the thermal radiative properties change between PFU fillet and top face, and this can also vary along the fillet. It is worth noting that it is difficult to accurately quantify which of the two contributors (angular distribution and normal emissivity value) dominates and in which proportion since these two parameters can impact the IR measurement in the same way. The simulation indicates a trend for grazing emission and/or lower emissivity for PFU top face. This study shows that PFU shaping and manufacturing, especially PFU with rounded bevel and/or chamfer, can impact the IR interpretation and the thermal radiative change on edge could be confused with false hot spots. However, sharp edges should be less impacted. Moreover, a similar light pattern has been observed on the fillet of AUG inner target, as shown in Fig. 6. In this case, a non-uniform emissivity model between PFU top face and its edge is not sufficient to explain the luminous trail. At this stage, other hypotheses are under investigation, such as tiles misalignments and variable fraction of wetted surface toroidal face.

5.3. Towards Infra-red quantitative thermography

As shown in the previous section, photonic simulation is a remarkable tool to discriminate real thermal events from reflection patterns and to investigate the origin of unpredicted light patterns. From this photonic simulation, it is then possible to evaluate the photon flux emitted by each surface. The further challenge is the IR quantitative thermography aiming at determining the true surface temperature by solving unknow emissivity and additional parasitic flux coming from reflections within fully radiative and metallic environment. Furthermore, due to the correlation between emissivity and temperature, it will be not possible to estimate these two parameters simultaneously without approximations and assumptions which will potentially affect the accuracy of
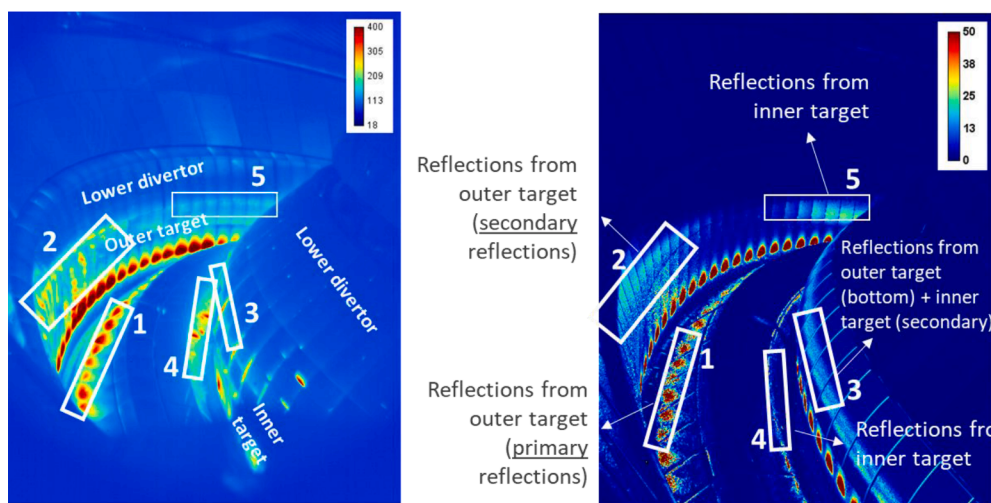

Fig. 6. (Left figure): Experimental IR image (in Digital Level) of AUG (Pulse #32858, IR camera (sector 9) (Right image) Simulated image considering highly reflectance materials (in radiance unit).
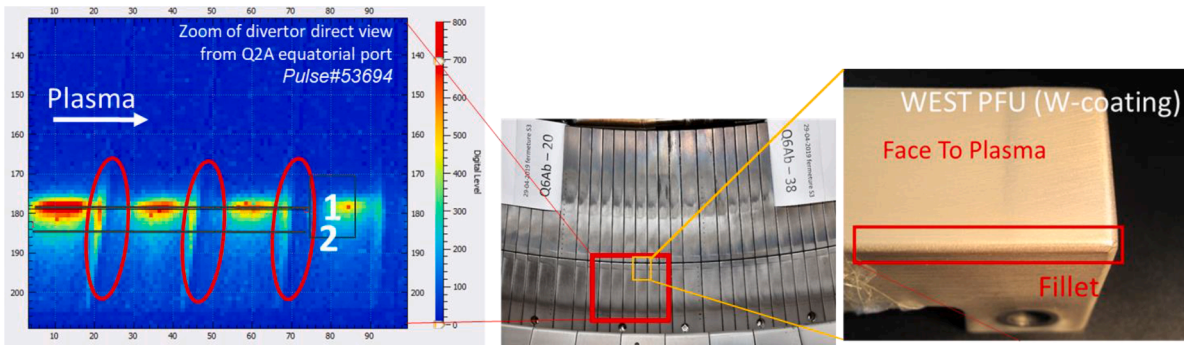
Fig. 7. (Left figure) Zoom of WEST divertor direct view from Q2A equatorial port: unexpected light pattern is observed along the rounded bevel of WEST inertial PFU (trailing edge) (Middle figure) Picture of WEST lower divertor (Right Figure) Zoom on inertial WEST PFU with a rounded bevel.
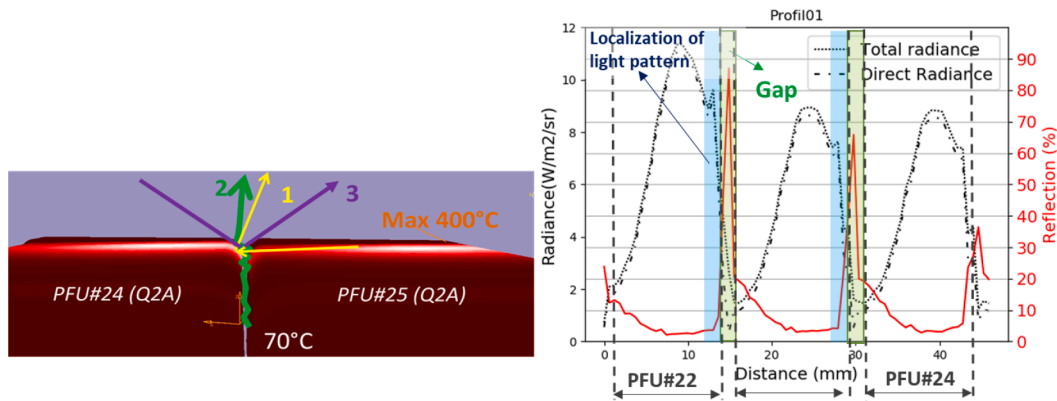

Fig. 8. (Left Figure) Illustration of different possible reflection contributions: (1) light coming from adjacent PFU at 400 °C and reflected by bevel, (2) multiple reflections between lateral faces of PFU at 70 °C and (3) other contributions coming from in to vessel components out of camera views. (Right Figure) Simulated radiance profile along three WEST inertial PFU. The dashed black curve is the total radiance collected by the camera. Dash-dotted black curves are the direct radiance, i.e., the flux emitted by the target and collected by the camera without reflections. The comparison of total and direct radiance gives the part of reflected flux (red curve), which is not significant enough on the region where is localized the light pattern (blue area) predicted between 5 and 20%. Green area indicate the gap between PFU. (For interpretation of the references to colour in this figure legend, the reader is referred to the web version of this article.)
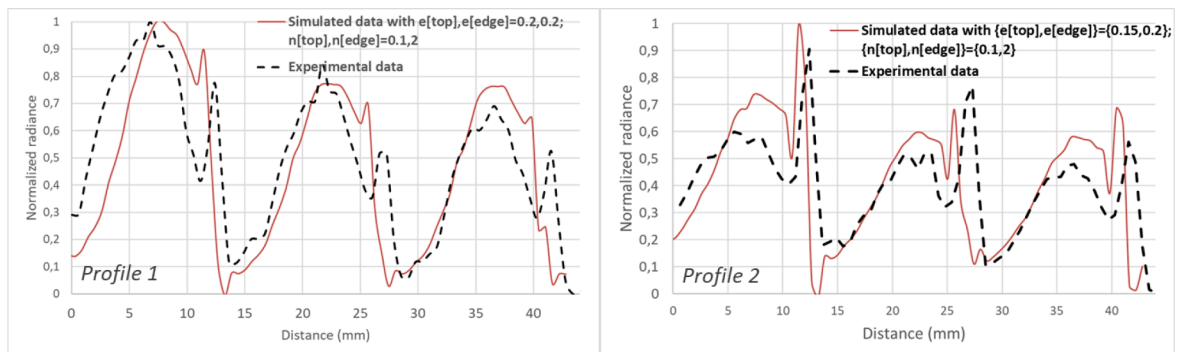

Fig. 9. Simulated and experimental profiles along three WEST inertial PFU, as illustrated in Fig. 7(x-axis indicates the position in mm from PFU#22). (Left figure): Profile 1 on maximum heat load (Right figure): Profile 2 below the maximum heat load. Dotted black curves are the experimental data, red curves the simulated ones. The experimental profiles (black curves) fit roughly with simulated profiles by changing the thermal radiative properties (normal emissivity e and n-power of intensity diagram emission model) along the PFU fillet. (For interpretation of the references to colour in this figure legend, the reader is referred to the web version of this article.)

temperature estimation. The proposed method takes places in two phases: (1) target emissivity is retrieved from thermal scene assuming known and uniform temperature, for example, during wall conditioning baking experiments or between pulses (2) target surface temperature is retrieved during plasma scenario assuming emissivity known. Both use inversion algorithms to retrieve thermal scene parameters (emissivity ε or surface temperature T_{surf}) from radiance collected by the camera by

solving the reflected flux. The inversion method consists in comparing, using least squares minimization method, experimental image and simulated image computed from forward model. In this case, Monte Carlo ray-tracing code is not adapted to compute fast enough the synthetic image and be used in iterative loop (10 h with 4 cores to generate a synthetic image with ~7% precision). This lead to develop reduced forward model able to compute quickly the IR images under some
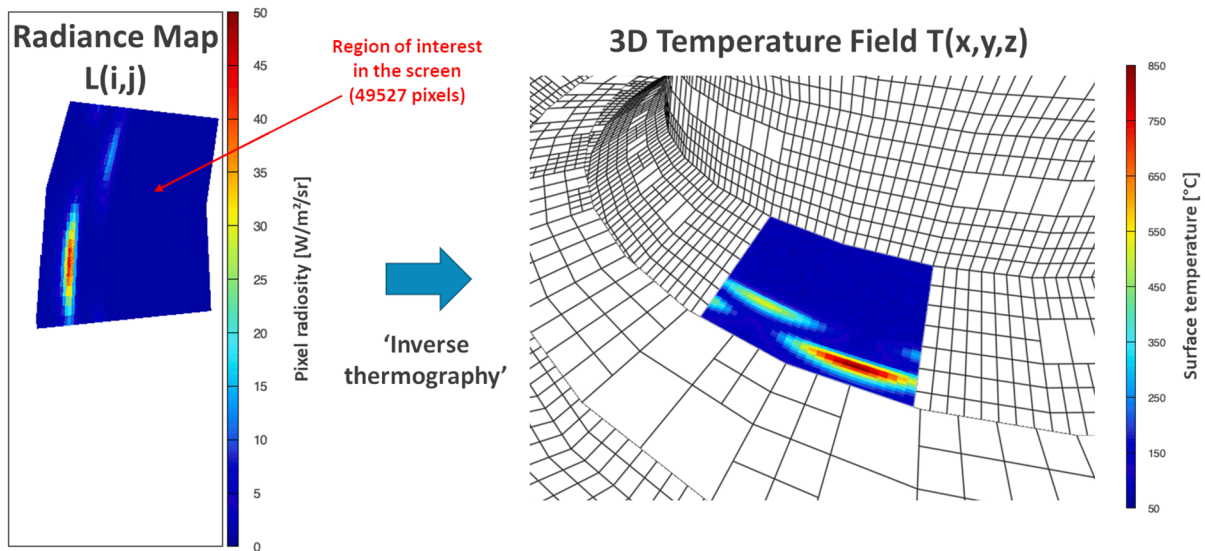
Fig. 10. (Left Figure) Noisy IR synthetic image in radiance unit L(i,j) including reflection coming from the surrounding environment (Right figure) 3D temperature field T(x,y,z) recovered after filtering reflection using inverse thermography method in WEST.

assumptions and approximations (dealing with only diffuse surface and simple geometry at this stage). Such a reduced photonic model is based on (1) the radiosity equations to compute the emittance (leaving flux) of each elementary surface (x,y,z) in the 3D scene taking into account multiple reflections and (2) a camera projection model to compute the radiance collected by each pixel (i,j). Fig. 10 shows an example of an "inverse thermography" application in WEST, which allows retrieving the 3D temperature field after filtering the reflection from an IR synthetic image. Encouraging results have been obtained on WEST tokamak prototype (with simplified geometry): target emissivity and surface temperature on lower divertor are recovered respectively with an error of 6% and better than 3% after solving the reflections and this, in short time (~10 s) [18]. Another step has been achieved using hierarchical methods to process more complex geometry [19,20]. It is worth noting that inversion method has been first tested in an inverse crime situation: experimental data have been replaced by synthetic data generated from the same forward model used for inversion, with an additive Gaussian white noise. Before testing method with real experimental data, intermediate step will be to generate new synthetic image with Monte Carlo ray tracing code dealing with specular surface and evaluate the error on temperature estimated from forward model dealing only diffuse surface. Further step will be to develop extended forward method able to manage specular surface.

6. Conclusion

Assessing accurately the impact of the radiative metallic environment is crucial both for machine protection and physics studies based on infra-red measurements. In this context, the interpretation of IR image is not straightforward as it is difficult to intuitively anticipate photon behavior in complex geometry with changing optical materials properties, wide camera view. Ray tracing simulation is a remarkable tool to reduce the risk of misleading interpretation and improve our understanding. Applied to WEST & AUG, this allowed discriminating both the real heat load deposition from false hot spots, while demonstrating the potential impact of variable emission model on PFU fillet. In parallel, several laboratory experiments have been conducted to establish a comprehensive model of the material emission and reflectance as a function of roughness, temperature, wavelength, machining. Before being exposed, it is found that the tungsten emissivity ranges around 0.1–0.2 at 4 μm with low temperature dependence. These laboratory experiments have proven the angular dependency of tungsten and a highly specular response of reflectance, which has been confirmed by

comparing simulated and experimental images in WEST and AUG. Moreover, these measurements also reveal that the behavior of emission and reflectance varies significantly with sample roughness and machining process. This has been confirmed with experiments in WEST and AUG, showing that thermal optical properties of materials change as the tests progress. Monitoring these modifications is required, which is more challenging without direct access to in-vessel components. Simulations coupled with dedicated experiments are essential. From a numerical prototype, it is shown that target emissivity value can be recovered from a controlled vessel baking scene (with uniform and known temperature) using an inverse thermography method for filtering reflections. Finally, achieving automatized and robust IR quantitative measurements for ITER remains a major challenge and experiments in current devices such as AUG and WEST are needed to test, improve and validate the methods.

CRediT authorship contribution statement

M-H. Aumeunier: Conceptualization, Methodology, Formal analysis, Investigation, Writing - original draft, Writing - review & editing. **J. Gerardin:** Formal analysis, Investigation, Writing - review & editing. **C. Talatizi:** Formal analysis. **M. Le Bohec:** Formal analysis, Writing - review & editing. **M. Ben Yaala:** Investigation, Formal analysis, Writing - review & editing. **L. Marot:** Validation, Formal analysis, Writing - review & editing. **T. Loarer:** Validation, Writing - review & editing. **R. Mitteau:** Investigation, Writing - review & editing. **J. Gaspar:** Writing - review & editing. **F. Rigollet:** Writing - review & editing. **X. Courtois:** Writing - review & editing. **M. Houry:** Writing - review & editing. **A. Herrmann:** Validation, Writing - review & editing. **M. Faitsch:** Writing - review & editing. **: . : .**

Declaration of Competing Interest

References

[1] A. Herrmann, et al., Plasma Phys. Control. Fusion 37 (1995) 17.
[2] M. Jakubowski, et al., Rev. Sci. Instrum. 89 (2018) 10E116.
[3] D. Guilhem, et al., Fusion Eng. Des. 74 (2005) 879–883.
[4] J. Bucalossi, et al., Fusion Eng. Des. 89 (2014) 907–912.
[5] A. Herrmann (Guest), Fusion Sci. Technol. 44 (3) (2003) 1–747.
[6] X. Courtois, et al., Fusion Eng. Des. 146 (2019) 2015–2020.
[7] R. Reichle, et al., Rev. Sci. Instrum. 81 (2010) 10E135.
[8] https://www.ansys.com/products/optical/ansys-speos.
[9] M. Firdaouss, et al., Fusion Eng. Des. 98–99 (2015) 1294–1298.
[10] J. Gérardin, et al., J. Phys. Conf. Ser. 745 (2016), 032019.
[11] J. Gérardin, et al., Congrès Français de Thermique (2017) 567–574.
[12] M. Ben Yaala et al., "Bidirectional reflectance measurement of tungsten samples to assess reflection model in WEST tokamak" to be submitted in Review of Scientific Instruments (2020).
[13] J. Gaspar, et al., Fusion Eng. Des. 146 (2019) 757–760.
[14] D.R. Lide, H.P.R. Frederikse (Eds.), CRC Handbook of Chemistry and Physics 75th edn Boca Raton, CRC Press, FL, 1994.
[15] M.A. Bramson, Infrared radiation a handbook for application, Opt. Phys. Eng. (1968).
[16] V. Basiuk, et al., Nucl. Fusion 41 (5) (2001) 477–485.
[17] B. Sieglin, et al., Rev. Sci. Instrum. 86 (2015), 113502.
[18] C. Talatizi, et al., Fusion Eng. Des. 159 (2020), 111867.
[19] M. Le Bohec et al., Congrès Français de Thermique 2019, hal-02905701.
[20] M. Le Bohec, et al., Congrès Français de Thermique (2020), https://doi.org/10.25855/SFT2020-073.